Aircraft System Identification from Multisine Inputs and Frequency Responses

Jared A. Grauer*
NASA Langley Research Center, Hampton, Virginia, 23681

Matthew J. Boucher†
NASA Armstrong Flight Research Center, Edwards, California, 93523

A frequency-domain approach is described for estimating parameters, such as stability and control derivatives, in aircraft flight dynamic models from measured input and output data. The approach uses orthogonal phase-optimized multisines for moving the aircraft control effectors, Fourier analysis for computing multiple-input multiple-output frequency responses, and a maximum likelihood estimator called frequency response error (FRE) for determining values and uncertainties for the model parameters. The approach is demonstrated using flight test data for two subscale airplanes: the T-2 generic transport model and the X-56A aeroelastic demonstrator. Results and comparisons with the output-error method indicated that the approach produced accurate estimates of stability and control derivatives and their uncertainties from flight test data.

I. Nomenclature

a_z	=	vertical accelerometer measurement, g
b	=	wing span, ft
$\bar{c}$	=	mean aerodynamic chord, ft
$E[.]$	=	expectation operator
g	=	gravitational acceleration, ft/s^2
$\mathbb{I}$	=	identity matrix
I_{xx}, I_{yy}, I_{zz}, I_{xz}	=	moments and product of inertia, slug-ft^2
j	=	imaginary number, = $\sqrt{-1}$
m	=	aircraft mass, slug
q	=	pitch rate, rad/s
$\bar{q}$	=	dynamic pressure, lbf/ft^2
S	=	wing reference area, ft^2
$s(\hat{\theta})$	=	standard error
t	=	time, s
V	=	true airspeed, ft/s
Z, M, Q	=	vertical force, pitching moment, and generalized moment
α	=	angle of attack, rad
δ	=	control surface deflection, rad
$^{-1}$	=	matrix inverse
†	=	complex conjugate transpose
$\hat{}$	=	estimated value
$\dot{}$	=	time derivative

*Research Engineer, Dynamic Systems and Control Branch, MS 308, Associate Fellow AIAA.
†Research Engineer, Controls and Dynamics Branch, MS 4840D, Member AIAA.

II. Introduction

The identification of aircraft flight dynamics is often performed using frequency responses, which are nonparametric models describing the steady-state magnitude and phase changes of sinusoidal inputs passing through a linear time-invariant (LTI) system, as a function of frequency. Frequency responses are computed from measured input and output data, and then model parameters, such as stability and control derivatives, are estimated to best fit a parametric model to the empirical frequency response data. The popularity of this approach is due to many reasons including the familiarity of engineers with frequency responses, a number of theoretical and practical advantages under specific conditions, and the availability of software packages.

More specifically, a common and standardized approach for identification from frequency responses can be briefly summarized as the following basic procedure: (1) apply frequency sweeps to single inputs, (2) estimate frequency responses using spectral methods, and (3) identify model parameters by fitting a postulated linear dynamic model to data shown as Bode plots using a nonlinear optimization. Enhancements of this basic approach are discussed in Ref. [1].

A different excitation input, known as orthogonal phase-optimized multisines [2], has become prevalent in aircraft flight testing because of the ability to excite multiple inputs simultaneously, which can reduce flight test time and costs. References [3–6] have explored identification using these inputs and the spectral estimation approach. In contrast, Refs. [2, 7–9] proposed analyzing this data using Fourier analysis to compute frequency responses, rather than spectral estimation, and demonstrated real-time monitoring of stability margins and fault detection. In Ref. [10], this approach was extended to account for the effects of feedback and mixing on the bare-airframe frequency response estimates, which describe the dynamics between the control surfaces and the response of the aircraft. In Ref. [11], maximum likelihood estimation was applied to frequency response data of open-loop aircraft to estimate parameters in transfer function and state-space models. In each of these works, one portion of the identification analysis using multisine inputs and frequency responses was extended.

In this work, the individual contributions in Refs. [2, 7–11] are combined in a unified approach for system identification using multisine inputs and frequency responses. The approach consists of perturbing the inputs using multisines, computing frequency responses using Fourier analysis, and then identifying model parameters and uncertainties using a maximum likelihood estimator.

This paper is organized as follows. Section III defines the problem statement. Section IV provides context by briefly summarizing aircraft identification methods using frequency responses. Section V presents the proposed approach, consisting of experiment design, frequency response computation, and parameter estimation. Two examples using flight test data demonstrate the approach in Section VI. The first example is relatively simple and includes short period dynamics having one input and two outputs. The second example is more complicated and includes aeroelastic dynamics, multiple inputs and outputs, a feedback control law, and mixing of the control inputs. Section VII summarizes the conclusions of the paper.

III. Problem Statement

Frequency response identification methods assume an LTI system. For aircraft flight dynamics, this requirement usually leads to small-perturbation models about a reference flight condition. Under these assumptions, the postulated dynamic model can be represented as the canonical state-space structure

$$\dot{\mathbf{x}}(t) = \mathbf{A}\,\mathbf{x}(t) + \mathbf{B}\,\mathbf{u}(t) \tag{1a}$$

$$\mathbf{y}(t) = \mathbf{C}\,\mathbf{x}(t) + \mathbf{D}\,\mathbf{u}(t) \tag{1b}$$

where $\mathbf{u}$ is a vector of n_u inputs, $\mathbf{x}$ is a vector of n_x states, and $\mathbf{y}$ is a vector of n_y outputs. The matrices $\mathbf{A}$, $\mathbf{B}$, $\mathbf{C}$, and $\mathbf{D}$ have constant elements and include the model parameters to be estimated, such as stability and control derivatives.

The state-space model can alternatively be represented as an input-output transfer function matrix. This representation is obtained by assuming zero initial conditions, applying the Laplace transform to Eq. (1), eliminating the state variable, and rearranging as

$$\mathbf{H}(s) = \frac{\mathbf{y}(s)}{\mathbf{u}(s)} = \mathbf{C}\,(s\mathbb{I} - \mathbf{A})^{-1}\,\mathbf{B} + \mathbf{D} \tag{2}$$

In Eq. (2), $s = \sigma + j\omega$ is the Laplace variable and $\mathbf{H}(s)$ is an $n_y \times n_u$ matrix of transfer functions $H_{ij}(s)$ between input u_j and output y_i, for $i = 1, 2, \ldots, n_y$ and $j = 1, 2, \ldots, n_u$. Equation (2) is equivalent to Eq. (1) and is a complete description of the system model, except that it assumes initial conditions are zero.

Letting $\sigma = 0$ so that $s = j\omega$ simplifies the Laplace transform to the Fourier transform, which is a mapping of the system dynamics onto steady sinusoids. This simplification discards information about the transient response of

the system and retains only the steady-state response. Applying the Fourier transform to Eq. (2) yields the frequency response of the system

$$\mathbf{H}(j\omega) = \frac{\mathbf{y}(j\omega)}{\mathbf{u}(j\omega)} = \mathbf{C}\left(j\omega\mathbb{I} - \mathbf{A}\right)^{-1}\mathbf{B} + \mathbf{D} \tag{3}$$

The complex-valued frequency response is often visualized as a Bode plot, where the magnitude and phase components

$$\|H_{ij}(j\omega)\| = 20\,\log_{10}\sqrt{\Re[H_{ij}(j\omega)]^2 + \Im[H_{ij}(j\omega)]^2} \tag{4a}$$

$$\angle H_{ij}(j\omega) = \frac{180}{\pi}\arctan\left(\frac{\Im[H_{ij}(j\omega)]}{\Re[H_{ij}(j\omega)]}\right) \tag{4b}$$

are shown as a function of frequency. In Eq. (4), $\Re$ and $\Im$ indicate real and imaginary parts of a complex number, and the Bode magnitude and phase components have units dB and deg, respectively. Although the frequency response only characterizes the steady-state response of the system, it nonetheless contains all the information necessary to constitute the transfer function matrix in Eq. (2).

The problem considered in this paper is obtaining a parametric model of the aircraft from nonparametric frequency responses. First, $\mathbf{H}(j\omega)$ is computed using measurements of $\mathbf{u}(t)$ and $\mathbf{y}(t)$. Second, stability and control derivatives in $\mathbf{A}$, $\mathbf{B}$, $\mathbf{C}$, and $\mathbf{D}$ are determined that best match the model frequency response to the empirical frequency response data.

IV. Historical Perspectives

An early approach to identification, called the frequency approach, involved sine dwell experiments where a sinusoidal input would develop the steady-state response after transients decayed [12]. Comparison of input and output time histories resulted in the relative magnitude and phase at that frequency — one point on a Bode plot. The first reported application for aircraft was Ref. [13], where the elevator was oscillated and sensor response data were recorded. This process was repeated for several frequencies, inputs, and flight conditions to construct Bode plots in a simple and intuitive but time-consuming process.

Afterwards, the Fourier approach to frequency response estimation was investigated in Refs. [14–16]. Arbitrary inputs, such as pulses, steps, and square waves were applied by the pilot, and then frequency responses were calculated as a ratio of output-to-input Fourier transform data, as in Eq. (3). This approach used shorter durations of flight data than in the frequency approach, and the analysis was automated. However, several shortcomings were identified including errors resulting from transient responses in the data, lack of input power at some frequencies, susceptibility to random disturbances, and inaccuracies stemming from short time records [17, 18].

In the spectral approach, spectral density functions are first estimated from input and output data, and then frequency responses and coherence functions are computed [1, 19, 20]. This approach has become standard practice for identifying aircraft models from frequency responses and can be used with arbitrary inputs. As noted in Ref. [18], piloted inputs of increasing frequency, called frequency sweeps, can produce good modeling data if the frequency is increased slowly. The analysis however requires the selection of various parameters, such as window size, shape, and overlap.

Once empirical frequency response data are obtained, a model structure can be postulated and unknown parameters in that model determined. In early works, straight-line approximations and "elementary factors" were used to fit models to Bode plots [21, 22]. Reference [17] suggested using a nonlinear optimizer to match frequency responses. A similar strategy was used in Ref. [23] to estimate parameters that fit data on a Bode plot, which was used for SISO systems and included tunable weights for trading accuracy between the Bode magnitude and phase fits. An enhanced version of this approach using many different transfer functions is described in Ref. [1]. The identification of model parameters by fitting frequency response data was formalized for the maximum likelihood estimator in the frequency domain by Refs. [2, 24].

The approach described in the next section applies previously-developed, efficient, and effective modern methods for the experiment design and frequency response estimation. These modern methods are conceptually related to sine dwell testing and the Fourier approach to frequency response estimation, respectively.

V. Method

A. Experiment Design

The first step of the identification procedure is to obtain informative flight test data from which to extract the system model. The excitations used here are orthogonal phase-optimized multisines, hereafter referred to as multisines, which were developed in Refs. [25, 26] and are further discussed in Ref. [2].

Multisines are designed for a time duration T, which corresponds to a fundamental frequency $1/T$ and harmonic frequencies k/T for integer values of k. A set K of n_f harmonic frequencies is selected over the bandwidth of interest. The frequency spacing is determined by T, where a longer record length increases the frequency resolution and decreases the lowest attainable frequency. Good modeling results usually need at least two cycles of each frequency, making $k = 2$ a practical lower limit, although higher values are preferable for increased rejection of random errors. When there are multiple inputs to be excited simultaneously, K is divided into the subsets K_j each having n_{f_j} frequencies.

Once the harmonics have been selected and assigned, each of the n_u multisines is constructed as the sum of sinusoids

$$\mu_j(t) = \sum_{k \in K_j} a_k \sin\left(\frac{2\pi k}{T} t + \phi_k\right) \tag{5}$$

The amplitudes a_k form the power spectra of the multisines, and can be scaled to adjust the signal-to-noise ratios of the responses. The phase angles ϕ_k are optimized for minimum relative peak factor (RPF) to keep the aircraft near the reference flight condition. For modeling the bare-airframe dynamics, these inputs are added to the actuator commands, after any feedback or mixing and just before software position and rate limiters.

Multisines are well suited for frequency response estimation. First, all inputs are moved at the same time but in orthogonal ways. For modern aircraft with multiple control effectors, multisines can save time and cost in comparison to other inputs that are applied to individual control effectors one at a time. Second, the optimization used to determine phase angles creates relatively small responses, which is important for linear analysis techniques. Third, multisines are similar to the classical sine-dwell tests mentioned in Section IV. The difference here is that instead of using a single frequency on a single input in sequence, many frequencies are used on multiple inputs at the same time. Last, the input spectrum is concentrated at a set of discrete and known frequencies, which facilitates a relatively simple procedure for computing the frequency responses using the Fourier approach, as mentioned in Section IV and further discussed in the next section.

B. Frequency Response Computation

The second step in the identification is to compute the frequency responses from measured data. This process starts by transforming measured time series into the frequency domain. The analytical tool for this task is the finite Fourier transform

$$z(j\omega) = \int_0^T z(t)\, e^{-j\omega t}\, dt \tag{6}$$

for a measured time-domain signal, $z(t)$. In batch post-flight applications, Eq. (6) can be computed with high accuracy using a chirp z-transform with cubic interpolation of the measured data [2]. If the sampling frequency is much higher than the frequencies of interest, an Euler approximation of the integral can also be used, which enables a recursive formulation of the discrete Fourier transform for real-time estimation. Fourier transforms are only evaluated for the n_f frequencies in K because the system is assumed to be linear and the data are expected to be in steady-state oscillation, per Section III.

When there is no feedback of the outputs and no mixing between the inputs, each harmonic frequency in the multisine excitations is applied to a single input. Due to the assumed linearity of the system, the output responses at each harmonic frequency can then be uniquely attributed to the inputs. In this case, each frequency response can be computed as

$$H_{ij}(j\omega_k) = \frac{y_i(j\omega_k)}{u_j(j\omega_k)} \tag{7}$$

at the respective harmonic frequencies. This was the approach used in Refs. [2, 7–9].

When outputs are fed back to the inputs or when there is mixing of the control effectors after the excitations are applied, the harmonic frequencies are no longer applied to a single input, and the effects of the controls on the responses

are confounded. In this case, Eq. (7) may be generalized as a system of linear equations and partitioned as

$$\begin{bmatrix} \mathbf{A}_1 \\ \mathbf{A}_2 \end{bmatrix} \mathbf{h} = \begin{bmatrix} \mathbf{b}_1 \\ \mathbf{0} \end{bmatrix} \tag{8}$$

The $(n_y n_u n_f) \times 1$ element vector $\mathbf{h}$ contains all the frequency response evaluations at all harmonic frequencies. The matrix $\mathbf{A}_1$ contains Fourier transforms of the input data, and the vector $\mathbf{b}_1$ contains Fourier transforms of the response data. The second row of Eq. (8) contains interpolation equations which account for secondary contributions from the frequency responses. Equation (8) is square and sparse, and can be solved efficiently for the frequency response evaluations. In the absence of feedback and mixing, Eq. (8) reduces to Eq. (7). This was the approach used in Ref. [10].

Frequency response estimation using either Eq. (7) or (8) follows from the definition of the frequency response in Eq. (3) as the ratio of output and input Fourier transforms, similar to the Fourier approach discussed in Section IV. The current methodology is different than the traditional Fourier approach because the analysis is performed only at the harmonic frequencies known to be in the excitation input. This reduces the amount of computation and only uses the points with good signal-to-noise ratios. If the multisines are applied to multiple inputs simultaneously, the full transfer function matrix can be identified from a single maneuver. Furthermore, the analysis is simple and does not require selection of analysis parameters based on analyst experience or engineering judgment. Estimates are theoretically unbiased with errors that decrease as more data are collected [27, 28].

As with any approach based on frequency responses, results degrade in the presence of nonlinearities or time-varying dynamics, such as from fuel burn or variation in dynamic pressure. In addition, this technique is susceptible to atmospheric turbulence, which acts as an unmeasured input, or transient responses, which are not captured by the frequency response. However, because the multisines are a summation of steady sinusoids, the transient responses decay after the excitation onset. If needed, the excitation could be repeated, which also helps to reduce error from noise and disturbances. The general approach using Eq. (8) also degrades if the open-loop dynamics have lightly-damped modes and the multisine inputs were designed with a coarse frequency resolution. The coherence function, typically computed in a spectral analysis to determine the linearity of the input-output data, is always equal to unity and there is not informative with this approach because windows are not applied. However, if the experiment is conducted well and in calm air, the frequency response errors are generally white, normally distributed, and have constant statistics over frequency [10, 11].

C. Maximum Likelihood Parameter Estimation

The third step is to estimate parameters that best fit the frequency response of the model to the empirical frequency response data. The approach taken here is based on the maximum likelihood method developed in Refs. [2, 24] and applied in Ref. [11].

Consider the observation model for the computed frequency response data

$$\text{vec}\left[\mathbf{H}(j\omega_k)\right] = \text{vec}\left[\hat{\mathbf{H}}(j\omega_k)\right] + \mathbf{v}(j\omega_k) \tag{9}$$

where the vectorization operator vec[.] stacks the columns of the matrix argument to form a vector. In Eq. (9), $\mathbf{H}(j\omega_k)$ is the empirical frequency response data. and $\hat{\mathbf{H}}(j\omega_k)$ is the frequency response of the model in Eq. (3) for a given vector of model parameters, $\boldsymbol{\theta}$. The vector $\mathbf{v}(j\omega_k)$ are errors in the frequency responses and are assumed to be stationary, normally distributed, and spectrally white with

$$E\left[\mathbf{v}(j\omega_k)\right] = \mathbf{0} \tag{10a}$$

$$E\left[\mathbf{v}(j\omega_k)\,\mathbf{v}^{\dagger}(j\omega_k)\right] = \frac{1}{n_f}\,\mathbf{S}_{vv} \tag{10b}$$

The matrix $\mathbf{S}_{vv}$ is the spectral density of $\mathbf{v}(t)$ and is a fully-populated, complex-valued matrix because measurement noise on any particular input or output affects several frequency responses. The residuals $\boldsymbol{\nu} = \hat{\mathbf{v}}$ are the complex-valued frequency response errors, computed as

$$\boldsymbol{\nu}(j\omega_k) = \text{vec}\left[\mathbf{H}(j\omega_k)\right] - \text{vec}\left[\hat{\mathbf{H}}(j\omega_k)\right] \tag{11}$$

which quantify differences between the empirical data and the model at the frequencies in the multisine inputs.

The maximum likelihood estimator for this problem minimizes the cost

$$J(\boldsymbol{\theta}, \mathbf{S}_{\nu\nu}) = n_f \sum_{k \in K} \boldsymbol{\nu}^{\dagger}(j\omega_k)\, \mathbf{S}_{\nu\nu}^{-1}\, \boldsymbol{\nu}(j\omega_k) + n_f \ln |\mathbf{S}_{\nu\nu}| + n_f n_u n_y \ln\left(\frac{\pi}{n_f}\right) \tag{12}$$

Equation (12) is the negative log-likelihood function and depends on the unknown model parameters and the unknown frequency response error spectral density. Because the residuals minimized are errors in the frequency responses, this approach can be called the frequency response error (FRE) method. Simultaneous optimization of Eq. (12) with respect to both $\boldsymbol{\theta}$ and $\mathbf{S}_{\nu\nu}$ at the same time typically exhibits convergence problems. Rather, a successful strategy is to use a relaxation technique where the cost function is alternately optimized with respect to $\mathbf{S}_{\nu\nu}$ or $\boldsymbol{\theta}$, while holding the other constant, until results converge. For a given $\hat{\boldsymbol{\theta}}$, minimizing the cost function in Eq. (12) with respect to $\mathbf{S}_{\nu\nu}$ results in the analytical solution

$$\hat{\mathbf{S}}_{\nu\nu} = \sum_{k \in K} \boldsymbol{\nu}(j\omega_k)\, \boldsymbol{\nu}^{\dagger}(j\omega_k) \tag{13}$$

where the model residuals are computed using Eq. (11). Then for a given $\hat{\mathbf{S}}_{\nu\nu}$, minimizing the cost function in Eq. (12) with respect to $\boldsymbol{\theta}$ leads to the reduced cost function

$$J(\boldsymbol{\theta}) = n_f \sum_{k \in K} \boldsymbol{\nu}^{\dagger}(j\omega_k)\, \hat{\mathbf{S}}_{\nu\nu}^{-1}\, \boldsymbol{\nu}(j\omega_k) \tag{14}$$

which requires iteration using a nonlinear optimizer. For the Gauss-Newton method, the parameter update is

$$\hat{\boldsymbol{\theta}} = \hat{\boldsymbol{\theta}}_0 - \mathbf{M}^{-1} \frac{\partial J}{\partial \boldsymbol{\theta}} \tag{15}$$

from the previous estimate $\hat{\boldsymbol{\theta}}_0$. Starting values for the model parameters may come from other analyses or prior information. In Eq. (15),

$$\mathbf{M} = 2n_f\, \Re \left[\sum_{k \in K} \mathbf{S}^{\dagger}(j\omega_k)\, \hat{\mathbf{S}}_{\nu\nu}^{-1}\, \mathbf{S}(j\omega_k) \right] \tag{16}$$

is the Fisher information matrix,

$$\frac{\partial J}{\partial \boldsymbol{\theta}} = -2n_f\, \Re \left[\sum_{k \in K} \mathbf{S}^{\dagger}(j\omega_k)\, \hat{\mathbf{S}}_{\nu\nu}^{-1}\, \boldsymbol{\nu}(j\omega_k) \right] \tag{17}$$

is the local cost gradient, and

$$\mathbf{S}(j\omega_k) = \frac{\partial}{\partial \boldsymbol{\theta}} \mathrm{vec}\left[\hat{\mathbf{H}}(j\omega_k)\right] \tag{18}$$

is the frequency response sensitivity matrix obtained from analytical derivatives or numerical finite differences. The optimization is stopped when changes in the parameter estimates, cost function, cost gradient, and residual spectral density between iterations are sufficiently small.

The uncertainties in the parameter estimates are the Cramér-Rao bounds

$$\mathrm{cov}(\hat{\boldsymbol{\theta}}) = \boldsymbol{\Sigma} = \mathbf{M}^{-1} \tag{19}$$

where cov(.) is the covariance operator. The square-root of the diagonal terms are the parameter standard errors. Given an adequate model structure and accurate frequency response data, Eq. (19) is a realistic estimate of the parameter uncertainty levels and does not require correction factors.

The maximum likelihood approach can be applied to dynamic models parameterized by either transfer function matrices or state-space differential equations. Although in this paper the estimator is applied to frequency response data computed using the methods in Section V.B, the approach can be applied to any frequency response data, including those computed using spectral methods. Accuracy of the results will degrade if the errors do not have the characteristics assumed in Eq. (10).

It is often the case that prior information is available for some of the parameters. This is useful when combining results from other analyses or multiple maneuvers, or when there is not enough information present in the data to

accurately estimate all of the model parameters. In this case, Eqs. (14)–(16) are modified to account for the prior estimate and uncertainty, $\boldsymbol{\theta}_p$ and $\boldsymbol{\Sigma}_p$, as [2, 24]

$$J(\boldsymbol{\theta}) = n_f \sum_{k \in K} \boldsymbol{\nu}^\dagger(j\omega_k)\, \hat{\mathbf{S}}_{\nu\nu}^{-1}\, \boldsymbol{\nu}(j\omega_k) + n_f \left(\boldsymbol{\theta} - \boldsymbol{\theta}_p\right)^T \boldsymbol{\Sigma}_p^{-1} \left(\boldsymbol{\theta} - \boldsymbol{\theta}_p\right) \tag{20a}$$

$$\hat{\boldsymbol{\theta}} = \hat{\boldsymbol{\theta}}_0 - \left(\mathbf{M} + \boldsymbol{\Sigma}_p^{-1}\right)^{-1} \left[\frac{\partial J}{\partial \boldsymbol{\theta}} + \boldsymbol{\Sigma}_p^{-1} \left(\boldsymbol{\theta} - \boldsymbol{\theta}_p\right)\right] \tag{20b}$$

$$\mathbf{M} = 2n_f\, \Re \left[\sum_{k \in K} \mathbf{S}^\dagger(j\omega_k)\, \hat{\mathbf{S}}_{\nu\nu}^{-1}\, \mathbf{S}(j\omega_k)\right] + \boldsymbol{\Sigma}_p^{-1} \tag{20c}$$

Incorporating prior information in this way, which is possible because of the maximum likelihood formulation, is statistically consistent and can be more accurate than setting unidentifiable parameters to fixed values during the estimation. It is necessary, though, that the flight conditions be similar for each of the maneuvers, e.g., similar angle-of-attack range, so that the same dynamic model can be expected to adequately characterize all of the data.

Multiple maneuvers may be processed simultaneously to estimate a single set of model parameters for the entire data set, rather than individually for each maneuver. This is done by computing frequency response data for each maneuver, and then stacking them in Eq. (9) as separate frequency responses to be matched. In this case, $\mathbf{S}_{\nu\nu}$ has $(n_y n_u \times n_y n_u)$ block matrices along its diagonal and is zero elsewhere. The multisine inputs may contain different harmonic frequencies for each maneuver. After the corresponding model frequency responses are assembled, the estimation proceeds normally. If the model parameters are nondimensional stability and control derivatives, an accurate estimation can be performed for maneuvers conducted at different airspeeds, altitudes, or fuel weights.

VI. Flight Test Examples

Two flight test examples are presented in this section. The first example is comparatively simple, with one input, two outputs, and open-loop rigid-body dynamics. The second example is more complicated and involves multiple inputs and outputs, feedback and mixing of the inputs, and aeroelastic dynamics. The multisine input design, Fourier transform, and parameter estimation were performed using routines from the MATLAB®-based software package called System IDentification Programs for AirCraft, or SIDPAC [29].

A. T-2 GTM

The T-2 Generic Transport Model (GTM), which is pictured in Fig. 1, is a 5.5% dynamically-scaled version of a transport-type aircraft. The airplane is fully instrumented with research-quality hardware and was flown remotely using the NASA AirSTAR (Airborne Subscale Transport Aircraft Research) flight test facility. Geometry and nominal mass properties for the T-2 are listed in Table 1. The nominal flight condition considered was straight and level flight at about 4.5 deg angle of attack, 135 ft/s airspeed, and 1400 ft altitude.

Fig. 1 T-2 airplane (credit: NASA Langley Research Center).

The maneuvers included multisine perturbations added to the conventional elevator, aileron, and rudder control surfaces after the flight condition was captured. Each multisine was designed for $T = 10$ s and included 7 frequencies evenly spaced between 0.2–2.2 Hz in 0.3 Hz increments. Five repeated maneuvers with this input, flown in calm air

Table 1 T-2 geometry and nominal mass properties.

Symbol	Value	Unit
$\bar{c}$	0.915	ft
b	6.849	ft
S	5.902	ft^2
m	1.585	slug
I_{xx}	1.179	slug-ft^2
I_{yy}	4.520	slug-ft^2
I_{zz}	5.527	slug-ft^2
I_{xz}	0.211	slug-ft^2

during Flight 33, were examined. For simplicity, this example only used measurements of the elevator as input, and pitch rate and vertical accelerometer as outputs; lateral-directional inputs and outputs were ignored. Figure 2 shows measured time histories for one representative maneuver, which are small perturbations about the reference condition with high signal-to-noise ratios, which were above 25. The corresponding frequency response estimates, computed using Eq. (7), are plotted as solid markers in Fig. 3.

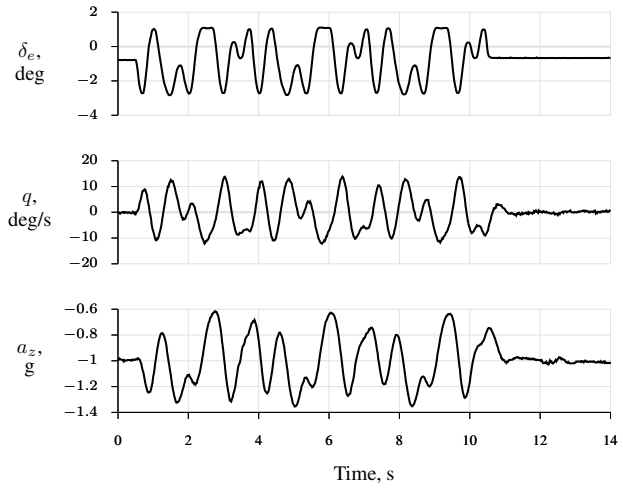

Fig. 2 T-2 flight test data, Maneuver 5.

The postulated dynamic model for parameter estimation was the simplified short-period approximation [2, 30]

$$\begin{bmatrix} \dot{\alpha} \\ \dot{q} \end{bmatrix} = \begin{bmatrix} Z_\alpha & 1 \\ M_\alpha & M_q \end{bmatrix} \begin{bmatrix} \alpha \\ q \end{bmatrix} + \begin{bmatrix} 0 \\ M_{\delta_e} \end{bmatrix} \delta_e \tag{21a}$$

$$\begin{bmatrix} q \\ a_z \end{bmatrix} = \begin{bmatrix} 0 & 1 \\ \frac{V}{g} Z_\alpha & 0 \end{bmatrix} \begin{bmatrix} \alpha \\ q \end{bmatrix} + \begin{bmatrix} 0 \\ 0 \end{bmatrix} \delta_e \tag{21b}$$

where the states, inputs, and outputs are perturbations from the reference condition. The derivatives Z_q and Z_{δ_e} were neglected, for simplicity. The estimated model parameters were the nondimensional stability and control derivatives, arranged as

$$\boldsymbol{\theta} = \begin{bmatrix} C_{Z_\alpha} & C_{m_\alpha} & C_{m_q} & C_{m_{\delta_e}} \end{bmatrix}^T \tag{22}$$

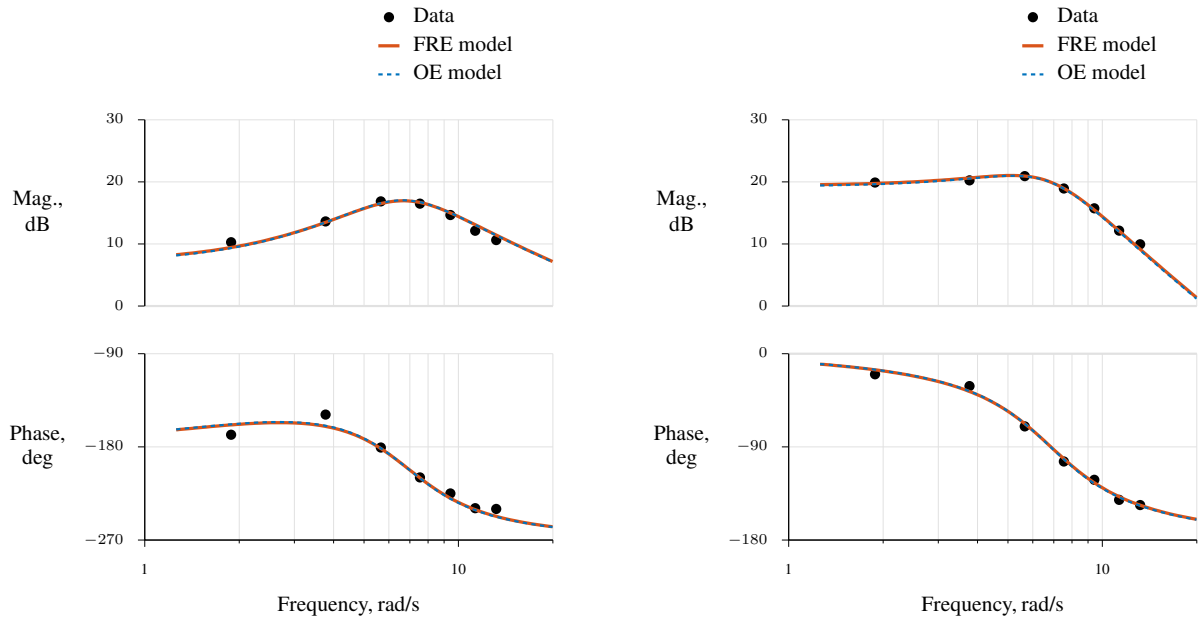

(a) q/δ_e.

(b) a_z/δ_e.

Fig. 3 T-2 frequency response estimates and identified models, Maneuver 5.

which are defined in terms of the dimensional stability and control derivatives as

$$Z_\alpha = \frac{\bar{q}S}{mV} C_{Z_\alpha} \qquad M_\alpha = \frac{\bar{q}S\bar{c}}{I_{yy}} C_{m_\alpha} \qquad M_q = \frac{\bar{q}S\bar{c}^2}{2VI_{yy}} C_{m_q} \qquad M_{\delta_e} = \frac{\bar{q}S\bar{c}}{I_{yy}} C_{m_{\delta_e}} \tag{23}$$

The empirical frequency response data shown in Fig. 3 was used to estimate the stability and control derivatives in the short period model. Bode plots for the model identified using the FRE approach, shown in Fig. 3 as solid red lines, closely matched the frequency response data. Starting values for the nonlinear optimization were taken from an equation-error (EE) analysis based on Fourier transform data [2], and results converged in 16 iterations. The identification used 14 data points in the frequency domain (7 harmonic frequencies for 2 frequency responses), which was significantly less than the 2103 measured samples available for a time-domain analysis.

For comparison, output error (OE) in the frequency domain was also used to estimate the stability and control derivatives in Eq. (21) by matching output Fourier transforms, based on the input measurements [2]. Frequencies between 0.15–2.5 Hz in 0.04 Hz increments were used for the analysis, resulting in 59 samples of Fourier transform data for each output. Bode plots for this identified model, shown as dashed blue lines in Fig. 3, are almost indistinguishable from the FRE results. From the same starting values, the OE analysis converged in 18 iterations.

Figure 4 shows parameter estimates and 2σ uncertainties for each of the five individual maneuvers using the FRE and OE approaches. Results obtained from FRE were in statistical agreement with the results obtained from OE. For each set of results, the observed scatter in the estimates was relatively small and within the estimated uncertainty. The scatter and uncertainty of these estimates could be further reduced by using additional output measurements, such as angle of attack and Euler pitch angle. These outputs were not included to keep this example simple, but have been used in other analyses [11].

Parameter estimates and standard errors from simultaneous analysis of all five maneuvers, treating frequency responses or response Fourier transforms from different maneuvers as separate outputs to be matched, are given in Table 2. The combined estimates are similar to those shown in Fig. 4 for the individual maneuvers, but had lower uncertainty bounds because more information was used in the estimation. Uncertainties were lower for the OE results because more frequencies were analyzed. All results were in statistical agreement between the two methods except for C_{Z_α}, due to omission of the C_{Z_q} and $C_{Z_{\delta_e}}$ derivatives from the model structure.

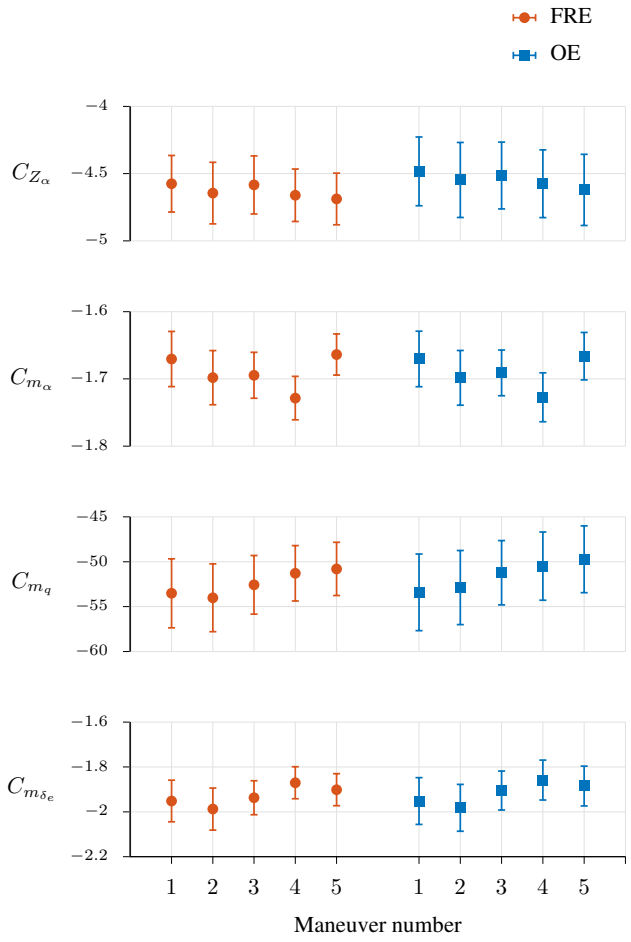

Fig. 4 T-2 parameter estimates from repeated maneuvers.

Table 2 T-2 parameter estimates using five maneuvers.

Parameter θ	FRE model $\hat{\theta} \pm s(\hat{\theta})$	OE model $\hat{\theta} \pm s(\hat{\theta})$
C_{Z_α}	-4.65 ± 0.05	-4.41 ± 0.02
C_{m_α}	-1.69 ± 0.01	-1.70 ± 0.00
C_{m_q}	-52.1 ± 0.75	-53.5 ± 0.35
$C_{m_{\delta_e}}$	-1.92 ± 0.02	-1.96 ± 0.01

B. X-56A MUTT

The X-56A MUTT (Multi-Utility Technology Testbed) aeroelastic demonstrator, which is pictured in Fig. 5, is also a subscale, remotely piloted airplane. Designed to study aeroelastic modeling and control technologies, the X-56A has an unstable aeroelastic mode within its normal flight envelope. The aircraft is highly instrumented and contains 10 independent trailing-edge control surfaces and many high-bandwidth sensors.

Fig. 5 X-56A airplane (credit: NASA / Jim Ross).

The reference condition for the maneuver examined was straight and level flight at approximately 58% of the flutter speed and 47% fuel weight. Five multisines were applied to each of the left-right symmetric pairs of control surfaces to excite the short period and first symmetric wing bending (SW1B) modes. Each multisine was designed to have a uniform power spectrum and included 25 harmonic frequencies.

Input and output modeling data for this maneuver are shown in Fig. 6 for one cycle of the multisine excitation. Numerical values were removed from the plots because the data are ITAR-restricted. The control surface deflections were measured with string potentiometers. The symmetric body flap pair, located furthest inboard, was denoted δ_{bfs}. The symmetric wing flap pairs, increasing in number towards the wing tip, were denoted δ_{wf1s}, δ_{wf2s}, δ_{wf3s}, and δ_{wf4s}. The pitch rate q^{gyr} was measured with a high-rate gyroscope mounted near the aircraft nose. Accelerations a_z^{cf} and a_z^{ca} were measured with vertical accelerometers installed in the fore and aft parts of the center body. Accelerations a_z^{smf}, a_z^{sma}, a_z^{sof}, and a_z^{soa} were measured with vertical accelerometers at the midspan fore and aft, and outboard fore and aft sections of the wings, respectively. Additional outputs were available for modeling but not used for this example. A diagram of sensor locations is shown in Fig. 7. The modeling data were small perturbations about the reference condition. For example, changes in airspeed were less than 0.5% and changes in mass were less than 0.4% over the duration of the maneuver.

Both a control law and mixer were active during this maneuver. Specifically, the flight path, pitch rate, and combinations of accelerometers were fed back to the inputs, and a virtual elevator command used δ_{wf2s} and δ_{wf3s} together. Therefore, Eq. (8) was used to compute the frequency responses, which are shown as black markers in Fig. 8. Known dynamics for the sensor models and low-pass filters were removed from the data using deconvolution in the frequency domain before the frequency responses were computed [31]. A total of 35 frequency responses were computed and used for identification. For clarity, only a subset of 6 frequency responses are shown, corresponding to the δ_{wf2s}, δ_{wf3s}, and δ_{wf4s} inputs, and q^{gyr} and a_z^{soa} outputs. Each row of Bode plots are plotted using the same vertical scales, and all plots use the same horizontal, logarithmic scale.

The postulated dynamics model for parameter estimation was a linear representation of the short period and SW1B

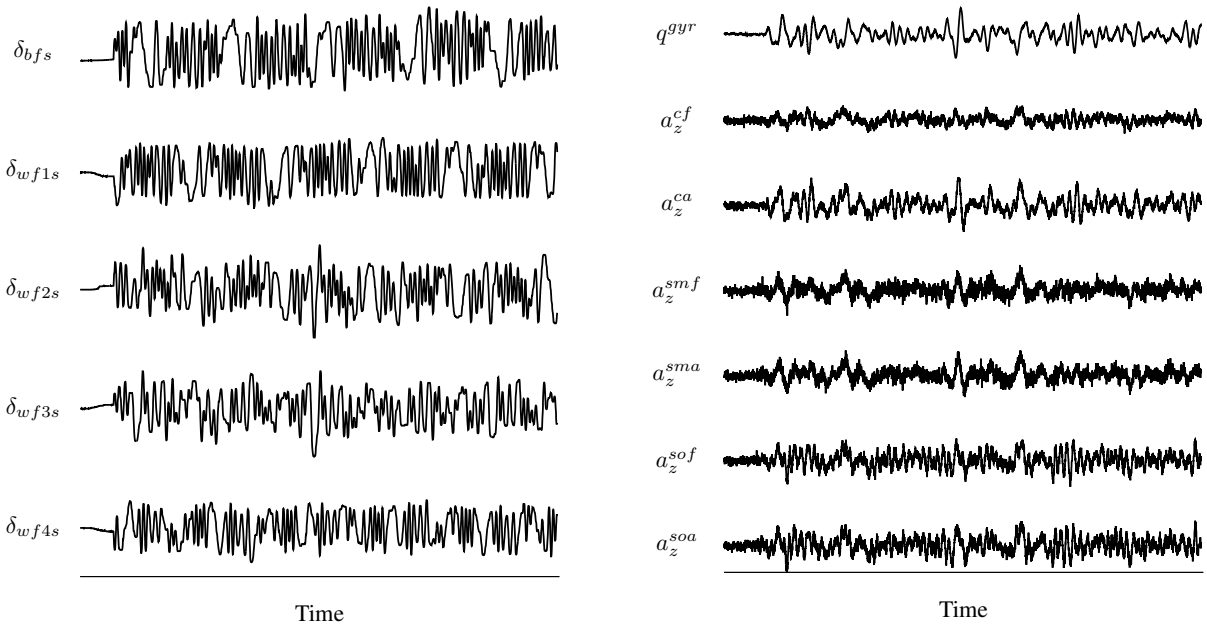

(a) Input data.

(b) Output data.

Fig. 6 X-56A measured flight test data (Phase 1, Flight 11, FTA 503).

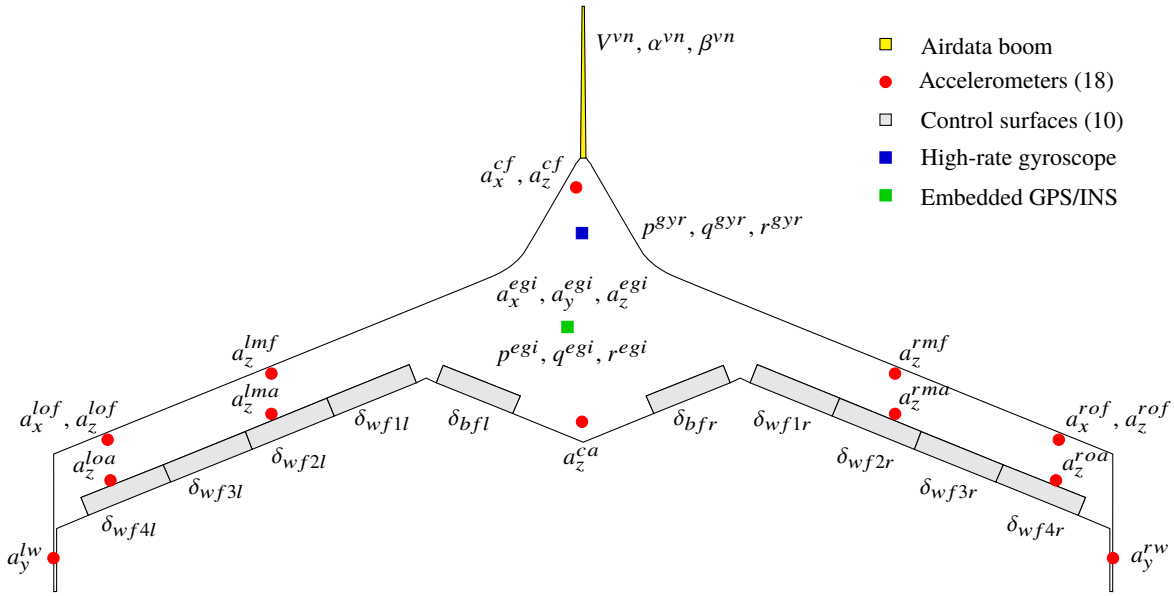

Fig. 7 X-56A planform with selected sensor and control surface locations.

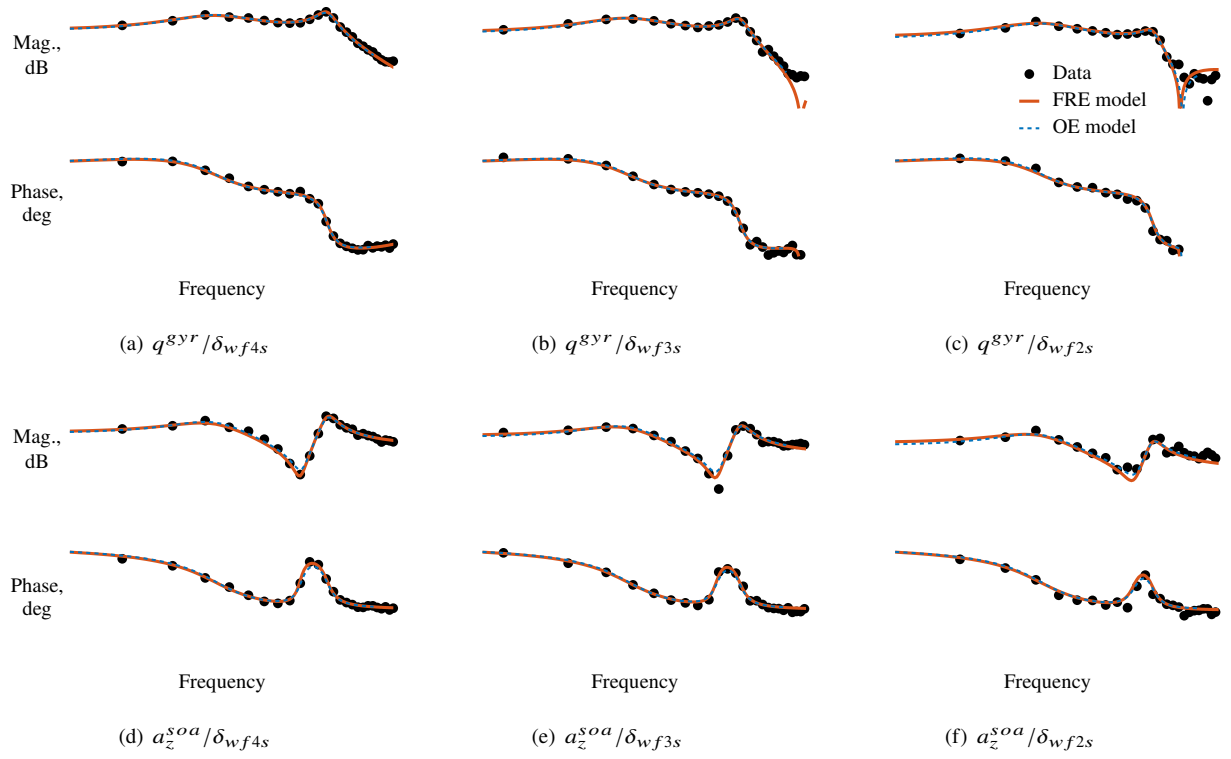

Fig. 8 X-56A frequency response estimates and identified models.

modes [32]

$$\begin{bmatrix} \dot{\alpha} \\ \dot{q} \\ \dot{\eta}_7 \\ \ddot{\eta}_7 \end{bmatrix} = \begin{bmatrix} Z_\alpha & 1+Z_q & Z_{\eta_7} & Z_{\dot{\eta}_7} \\ M_\alpha & M_q & M_{\eta_7} & M_{\dot{\eta}_7} \\ 0 & 0 & 0 & 1 \\ Q_{7_\alpha} & Q_{7_q} & Q_{7_\eta} - \omega_7^2 & Q_{7_{\dot{\eta}}} - 2\zeta_7\omega_7 \end{bmatrix} \begin{bmatrix} \alpha \\ q \\ \eta_7 \\ \dot{\eta}_7 \end{bmatrix} + \begin{bmatrix} Z_{\delta_{bfs}} & Z_{\delta_{wf1s}} & Z_{\delta_{wf1s}} & Z_{\delta_{wf1s}} & Z_{\delta_{wf1s}} \\ M_{\delta_{bfs}} & M_{\delta_{wf1s}} & M_{\delta_{wf1s}} & M_{\delta_{wf1s}} & M_{\delta_{wf1s}} \\ 0 & 0 & 0 & 0 & 0 \\ Q_{7_{\delta_{bfs}}} & Q_{7_{\delta_{wf1s}}} & Q_{7_{\delta_{wf1s}}} & Q_{7_{\delta_{wf1s}}} & Q_{7_{\delta_{wf1s}}} \end{bmatrix} \begin{bmatrix} \delta_{bfs} \\ \delta_{wf1s} \\ \delta_{wf2s} \\ \delta_{wf3s} \\ \delta_{wf4s} \end{bmatrix} \tag{24}$$

The state vector includes α and q, similar to Eq. (21), but also includes the generalized displacement η_7 and rate $\dot{\eta}_7$ of the SW1B genesis mode. The terms ω_7 and ζ_7 are the in-vacuo frequency and damping ratio of the SW1B mode, when no air is present, and were obtained from a finite element model (FEM) and ground vibration test (GVT), which is described more in Ref. [33]. The dimensional stability and control derivatives in Eq. (24) are defined in terms of the nondimensional versions as

$$Z_\alpha = \frac{\bar{q}S}{mV}C_{Z_\alpha} \quad Z_q = \frac{\bar{q}S\bar{c}}{2mV^2}C_{Z_q} \quad Z_{\eta_7} = \frac{\bar{q}S}{mV}C_{Z_{\eta_7}} \quad Z_{\dot{\eta}_7} = \frac{\bar{q}S\bar{c}}{2mV^2}C_{Z_{\dot{\eta}_7}} \quad Z_\delta = \frac{\bar{q}S}{mV}C_{Z_\delta} \tag{25a}$$

$$M_\alpha = \frac{\bar{q}S\bar{c}}{I_{yy}}C_{m_\alpha} \quad M_q = \frac{\bar{q}S\bar{c}^2}{2VI_{yy}}C_{m_q} \quad M_{\eta_7} = \frac{\bar{q}S\bar{c}}{I_{yy}}C_{m_{\eta_7}} \quad M_{\dot{\eta}_7} = \frac{\bar{q}S\bar{c}^2}{2VI_{yy}}C_{m_{\dot{\eta}_7}} \quad M_\delta = \frac{\bar{q}S\bar{c}}{I_{yy}}C_{m_\delta} \tag{25b}$$

$$Q_{7_\alpha} = \frac{\bar{q}S\bar{c}}{m_7}C_{Q_{7_\alpha}} \quad Q_{7_q} = \frac{\bar{q}S\bar{c}^2}{2Vm_7}C_{Q_{7_q}} \quad Q_{7_{\eta_7}} = \frac{\bar{q}S\bar{c}}{m_7}C_{Q_{7_{\eta_7}}} \quad Q_{7_{\dot{\eta}_7}} = \frac{\bar{q}S\bar{c}^2}{2Vm_7}C_{Q_{7_{\dot{\eta}_7}}} \quad Q_{7_\delta} = \frac{\bar{q}S\bar{c}}{m_7}C_{Q_{7_\delta}} \tag{25c}$$

where a short-hand notation has been used for the control surface derivatives. The generalized mass m_7 of the SW1B mode was also obtained from the FEM. The nondimensional stability and control derivatives in Eq. (25) were the unknown model parameters to be estimated.

The linearized output equations for the gyroscope and the i^{th} vertical accelerometer measurements in longitudinal flight are [34]

$$q^{gyr} = q + \nu_{7_\theta}^{gyr}\dot{\eta}_7 \tag{26a}$$

$$a_z^i = \frac{V}{g}(\dot{\alpha} - q) - \frac{x_a^i}{g}\dot{q} + \frac{\phi_{7_z}^i}{g}\ddot{\eta}_7 \tag{26b}$$

where x_a^i is the location of the accelerometer relative to the center of mass along the body x axis. The term $\nu_{7_\theta}^{gyr}$ is the angular pitch displacement of the SW1B mode at the gyroscope sensor, and $\phi_{7_z}^i$ is the vertical displacement of the SW1B mode at the accelerometer; both were obtained from the FEM.

Parametric models were identified using the frequency response data in Fig. 8, the dynamic model in Eq. (24), and the output equations in Eq. (26). Starting values for the model parameters in the nonlinear optimization came from an aeroelastic panel code solution [35]. In addition, time delays were estimated with the stability and control derivatives for each of the 7 output variables to correct for small phase errors due to measurement time skews, nonlinearities, and unmodeled higher-frequency dynamics. The models identified using FRE, shown in Fig. 8 using solid red lines, matched the obtained frequency response data well. The parameter values were near the starting values, within expected ranges, and had standard errors less than 12% of the parameter values. Frequency responses of another dynamic model, identified using OE to match Fourier transform data, are also shown in Fig. 8 using dashed blue lines. More details on the OE analysis can be found in Ref. [36]. In general, the fits using FRE and OE in the frequency domain were very close and produced similar parameter estimates.

VII. Conclusions

An approach for identifying dynamic models of aircraft from measured data was proposed. The aircraft dynamics are excited using orthogonal phase-optimized multisines, which are added to the input command path at the actuators and after any feedback or mixing. Frequency responses are computed as ratios of output to input Fourier transform data at the multisine harmonic frequencies. The maximum likelihood estimator is used to determine parameters and associated uncertainties in a given model structure that best match the model frequency responses to the frequency response data. Flight test examples demonstrated the approach using the short period dynamics of the T-2 generic transport model airplane flown in open loop, and the aeroelastic dynamics of the X-56A MUTT flown in closed loop with control input mixing.

The approach is based in frequency-domain analysis and therefore has advantages over time-domain analyses including high-frequency noise rejection, selection of the frequency range of interest, and efficient estimation. The use of multisine inputs allows for an efficient experiment where all of the inputs are excited at the same time but in orthogonal ways, which can save time and cost during flight tests. Computation of the empirical frequency responses, which provide additional physical insight into the dynamics and parameters of interest, are done in a simple and procedural manner without judgment or design parameter selections from the analyst. Using the maximum likelihood estimator provides favorable asymptotic properties of the estimates, produces statistically accurate uncertainties for the estimated parameters without further correction, and facilitates incorporating prior information and combining information from multiple maneuvers.

The approach, however, still has several limitations. Although frequency responses provide physical insight into the dynamics, their use restricts the modeling to linear, time-invariant systems, which in turn requires flight test data having small perturbations about a reference condition. Whereas other approaches can use shorter data records, accurate frequency response estimation requires steady-state data, which require longer time durations to develop. Additional cycles of steady-state data may be required if atmospheric turbulence or low signal-to-noise ratios are present. In addition, matching frequency responses, rather than measured output data, requires the indirect step of computing the frequency responses, which can introduce errors and degrade parameter estimates. Lastly, the approach requires the ability to add computerized inputs to the command path.

This approach is useful in identification of aircraft flight dynamics. Exciting all of the inputs simultaneously leads to shorter maneuver durations that save time and costs. The computation of frequency responses can provide additional insight into the model structure for parametric modeling, and can be used to obtain rough estimates of some parameters.

Parametric modeling of frequency responses can be done using transfer functions to obtain modal frequency and damping parameters, or using state-space models to identify stability and control derivatives. Subsets of frequency responses, for example from a single input, can be used to gradually develop the model and identify which parameters can be accurately estimated. Estimates using this approach can also be used to corroborate those from an equation-error or output-error analysis, which can use the same input-output modeling data.

Acknowledgments

This research was supported by the NASA Advanced Air Transport Technology (AATT) project. The T-2 flight data used was generated by the NASA Langley Research Center AirSTAR team under the NASA Aviation Safety Program, Vehicle Systems Safety Technologies (VSST) project. The X-56A flight data used was generated by the NASA Armstrong Flight Research Center X-56 team under the AATT project.

References

[1] Tischler, M., and Remple, R., *Aircraft and Rotorcraft System Identification: Engineering Methods with Flight Test Examples*, 2nd ed., AIAA, Reston, VA, 2012. doi:10.2514/4.868207.

[2] Morelli, E., and Klein, V., *Aircraft System Identification: Theory and Practice*, 2nd ed., Sunflyte, Williamsburg, VA, 2016.

[3] Young, P., and Patton, R., "Comparison of Test Signals for Aircraft Frequency Domain Identification," *Journal of Guidance, Control, and Dynamics*, Vol. 13, No. 3, 1990, pp. 430–438. doi:10.2514/3.25355.

[4] Heeg, J., and Morelli, E., "Evaluation of Simultaneous Multisine Excitation of the Joined Wing SensorCraft Aeroelastic Wind Tunnel Model," AIAA Paper 2011-1959, 2011. doi:10.2514/6.2011-1959.

[5] Ivler, C., Rowe, E., Martin, J., Lopez, M., and Tischler, M., "System Identification Guidance for Multirotor Aircraft: Dynamic Scaling and Test Techniques," VFS Paper 239, 2019.

[6] Lichota, P., Szulcyk, J., Tischler, M., and Berger, T., "Frequency Response Identification from Multi-Axis Maneuver with Simultaneous Multisine Inputs," *Journal of Guidance, Control, and Dynamics*, Vol. 42, No. 11, 2019, pp. 2550–2556. doi:10.2514/1.G004346.

[7] Grauer, J., and Morelli, E., "Method for Real-Time Frequency Response and Uncertainty Estimation," *Journal of Guidance, Control, and Dynamics*, Vol. 37, No. 1, 2014, pp. 336–343. doi:10.2514/1.60795.

[8] Grauer, J., "Aircraft Fault Detection using Real-Time Frequency Response Estimation," AIAA Paper 2016-0372, 2016. doi:10.2514/6.2016-0372.

[9] Morelli, E., and Grauer, J., "Practical Aspects of the Frequency Domain Approach for Aircraft System Identification," AIAA Paper 2018-3477, 2018. doi:10.2514/6.2018-3477.

[10] Grauer, J., and Boucher, M., "Real-Time Estimation of Bare-Airframe Frequency Responses from Closed-Loop Data and Multisine Inputs," *Journal of Guidance, Control, and Dynamics*, 2019. doi:10.2514/1.G004574.

[11] Grauer, J., "Dynamic Modeling using Output-Error Parameter Estimation based on Frequency Responses Estimated with Multisine Inputs," NASA TM-2018-220108, November 2018.

[12] James, H., Nichols, N., and Phillips, R., *Theory of Servomechanisms*, McGraw-Hill, New York, NY, 1947.

[13] Milliken, W., "Progress in Dynamic Stability and Control Research," *Journal of the Aeronautical Sciences*, Vol. 14, No. 9, 1947, pp. 493–519. doi:10.2514/8.1434.

[14] Seamans, R., Bromberg, B., and Payne, L., "Application of the Performance Operator to Aircraft Automatic Control," *Journal of the Aeronautical Sciences*, Vol. 15, No. 9, 1948, pp. 535–555. doi:10.2514/8.11644.

[15] Seamans, R., Blasingame, B., and Clementson, G., "The Pulse Method for the Determination of Aircraft Dynamic Performance," *Journal of the Aeronautical Sciences*, Vol. 17, No. 1, 1950, pp. 22–38. doi:10.2514/8.1514.

[16] LaVerne, M., and Boksenbom, A., "Frequency Response of Linear Systems from Transient Data," NACA TR-977, September 1950.

[17] Greenberg, H., "A Survey of Methods for Determining Stability Parameters of an Airplane from Dynamic Flight Measurements," NACA TN 2340, April 1951.

[18] Eggleston, J., and Mathews, C., "Application of Several Methods for Determining Transfer Functions and Frequency Response of Aircraft from Flight Data," NACA TR 1204, January 1954.

[19] Tukey, J., "The Sampling Theory of Power Spectrum Estimates," No. NAVEXOS-P-735 in Symposium on Applications of Autocorrelation Analysis to Physical Problems, Office of Naval Research, Woods Hole, MA, 1949.

[20] Bendat, J., and Piersol, A., *Random Data: Analysis and Measurement Procedures*, 2nd ed., John Wiley & Sons, New York, NY, 1986.

[21] Lees, S., "Graphical Aids for the Graphical Representation of Functions of the Imaginary Argument," MIT Engineering Memorandum E-25, February 1951.

[22] Bruns, R., and Saunders, R., *Analysis of Feedback Control Systems: Servomechanisms and Automatic Regulators*, McGraw-Hill, New York, NY, 1955.

[23] Hodgkinson, J., LaManna, W., and Heyde, J., "Handling Qualities of Aircraft with Stability and Control Augmentation Systems — A Fundamental Approach," *Aeronautical Journal*, Vol. 80, No. 782, 1976, pp. 75–81. doi:10.1017/S0001924000033510.

[24] Klein, V., "Aircraft Parameter Estimation in Frequency Domain," AIAA Paper 78-1344, 1978. doi:10.2514/6.1978-1344.

[25] Morelli, E., "Multiple Input Design for Real-Time Parameter Estimation in the Frequency Domain," IFAC Paper REG-360, 2003. doi:10.1016/S1474-6670(17)34833-4.

[26] Morelli, E., "Flight-Test Experiment Design for Characterizing Stability and Control of Hypersonic Vehicles," *Journal of Guidance, Control, and Dynamics*, Vol. 32, No. 3, 2009, pp. 949–959. doi:10.2514/1.37092.

[27] Ljung, L., *System Identification: Theory for the User*, 2nd ed., Prentice Hall, Upper Saddle River, NJ, 1999. doi:10.1109/MRA.2012.2192817.

[28] Pintelon, R., and Schoukens, J., *System Identification: A Frequency Domain Approach*, 2nd ed., John Wiley & Sons, Hoboken, NJ, 2012. doi:10.1002/9781118287422.

[29] Morelli, E., "System IDentification Programs for AirCraft (SIDPAC)," version 4.1, NASA Software Catalog, `http://software.nasa.gov`, accessed Oct. 2019.

[30] McRuer, D., Graham, D., and Ashkenas, I., *Aircraft Dynamics and Automatic Control*, Princeton University Press, Princeton, NJ, 1973.

[31] Grauer, J., and Boucher, M., "Frequency-Domain Deconvolution for Flight Dynamics Applications," AIAA Paper 2018-3157, 2018. doi:10.2514/6.2018-3157.

[32] Schmidt, D., *Modern Flight Dynamics*, McGraw Hill, New York, NY, 2012.

[33] Pak, C., and Truong, S., "Creating a Test-Validated Finite-Element Model of the X-56A Aircraft Structure," *Journal of Aircraft*, Vol. 52, No. 5, 2015, pp. 1644–1677. doi:10.2514/1.C033043.

[34] Grauer, J., and Boucher, M., "Output Measurement Equations for Flexible Aircraft Flight Dynamics," NASA TM-2018-220102, October 2018.

[35] Ouellette, J., "Aeroservoelastic Modeling of Body Freedom Flutter for Control Systen Design," AIAA Paper 2017-0019, 2017. doi:10.2514/6.2017-0019.

[36] Grauer, J., and Boucher, M., "Identification of Aeroelastic Models for the X-56A Longitudinal Dynamics Using Multisine Inputs and Output Error in the Frequency Domain," *Aerospace*, Vol. 6, No. 24, 2019, pp. 1–25. doi:10.3390/aerospace6020024.